Journal of Applied Polymer Science

Self-Assembled Nanoblends of Functional Polystyrene and a Reactive Aramid: Morphological and Thermomechanical Profile

Ayesha Kausar,[1,2] Sonia Zulfiqar,[3] Muhammad Ilyas Sarwar[1]

[1]Department of Chemistry, Quaid-i-Azam University, Islamabad 45320, Pakistan

[2]Nanosciences and Catalysis Division, National Centre for Physics, Islamabad, Pakistan

[3]Centre for Climate Research and Development, Department of Meteorology, COMSATS Institute of Information Technology, Islamabad 44000, Pakistan

Correspondence to: M. I. Sarwar (E-mail: ilyassarwar@hotmail.com)

ABSTRACT: Various blends composed of pure polystyrene (PS) and modified PS [amino-functionalized polystyrene (PS–NH_2)] were prepared with a new aromatic polyamide obtained through the polycondensation of 1,5-diaminonaphthalene and 1,4-phenylenediamine with isophthaloyl chloride. The variation in the morphological and thermophysical profiles in the two blend systems with aramid loading were investigated. The amine functionality introduced to PS enhanced its compatibility with the polyamide because of the formation of an aramid-*graft*-PS copolymer. The grafting, hydrogen bonding, and phenylene-ring (π–π) stacking between the chains of the two components finally nurtured self-assembled nanostructured blends. A strong compatibilizing effect was observed for the 50, 60, and 70 wt % aramid blends, where an exceptionally inimitable cocontinuous self-assembled morphology was formed by PS–NH_2/aramid. Significant developments in the morphology along with thermal and mechanical stability were observed for the reactive PS/aramid system. The most favorable mechanical and thermal data supported by the finest nanostructure were observed with 70 wt % polyamide addition. Future prospects may involve the formation of nanotemplates and nanostructured membranes. © 2013 Wiley Periodicals, Inc. J. Appl. Polym. Sci. **2014**, *131*, 39954.

KEYWORDS: compatibilization; morphology; self-assembly

Received 2 February 2013; accepted 9 September 2013

DOI: 10.1002/app.39954

INTRODUCTION

Nowadays, industries are increasingly trying to replace metal parts with polymer-based materials because of their lower density, easy maintenance, and low price; as a result, the use of polymer blends is hastily growing.[1] The blending of polymers provides an efficient way to develop new materials with tailored properties and has received much attention from academia and engineering. Through blending, several properties of polymers can be improved; however, the aspirations of polymer scientists to fabricate better products are often aggravated by the low compatibility of the blend components. Polymer blends usually proffer materials a spacious range of mechanical properties by fine-tuning the sort and amount of polymers in the mixture. Nevertheless, because of the immiscibility of the two polymers, blend components usually phase-separate into macroscopic domains; this yields poor mechanical properties, especially the tensile strength. The microstructure of uncompatibilized blends is coarse, irregular, and unstable with a sharp and weak interface, which ensures inferior physical characteristics in the immiscible blend. This phenomenon can be suppressed by the addition of an appropriate compatibilizer, which reduces the interfacial tension and leads to improved mechanical properties in the final blend. The fine interfacial adhesion ensured by the compatibilizer generally leads to the refinement and stabilization of blend morphology because it is quite significant for stress transfer between different phases and demonstrates an enhanced tensile strength. Therefore, compatibilization of polymer blends with various techniques has become an important feature of polymer science and technology.[2] Unfortunately, polymer–polymer blends exhibit properties (relatively low impact strength, low wear resistance, high friction, etc.) that are undesirable for demanding service conditions. Graft copolymers, containing blocks of the same chemical structure as the heterophases in an incompatible binary polymer blend, are capable of compatibilizing these polymer mixtures.[3,4] When localized at the interface between the immiscible polymers, these copolymers lower the interfacial tension and, thus, disperse the polymer blend into smaller domains because of reduced coalescence of the stabilized particles. In this regard, interfacial tensions have a crucial effect on the properties of multiphase systems.[5–10] Considerable

articles have been published in the literature on the attainment of desired properties by the formation of block copolymers.[11] A block copolymer containing different polymeric segments may generate microphases that cause a reduction in the size of the particles in the blend matrix. A weak aspect of most polymers is their poor physical properties; so much work is needed in this area.[12]

The self-assembly of polymers generating nanostructures has become one of the most prevalent research subjects in polymer science during recent decades.[13] Because of advances in the field of polymer synthesis, the effects of polymer architecture on the self-assembled morphology of complex macromolecules have been investigated. Among the different approaches to self-assembly, the patterning of graft/block copolymers has been studied extensively. The most astounding self-assembly, hence, has been observed in block copolymers. Constituent phases in these copolymers either separate macroscopically or mix molecularly according to classical Flory–Huggins theory.[14,15] The nanostructures in block copolymers include spheres, cylinders, gyroids, and lamellae. The self-assembly usually originates from the structure in which distinct blocks that are thermodynamically incompatible are covalently linked to form a single chain. Consequently, self-assembly in these block copolymers may be initiated through strong molecular interactions, such as hydrogen bonding.[16,17] If such strong molecular interactions are removed from the system, macrophase separation will appear. So miscible polymer blends are actually a system in which different thermodynamically incompatible molecules are linked to form strongly correlated chains by physical interaction. Many researchers have investigated the orientation behavior of block copolymers, with the most recent efforts being directed toward nanotechnologies. The self-assembly of block copolymers is especially pertinent to the control of the periodic nanostructures. Nanotechnological applications of graft/block copolymers are latent because of their substantial properties, including mechanical, electrical, and optical properties. These properties provide considerable advantages to nanostructure membranes, nanotemplates, photonic crystals, and high-density information storage media. In a variety of relevance, such nanopatterns need to be achieved as ordered and tunable structures.[18,19] Consequently, the control over the orientation of such structures with defect-free ordering on a large scale still exists as a key research challenge.

We have formulated and studied novel uncompatibilized and compatibilized compositions of polystyrene (PS) and aramid blend systems. Efforts have recently been directed toward high-performance blends for use in place of metals in industries such as the automotive and aviation industries, which demand high-performance parts. Among polymer-based materials,[20] those based on PS[5,21,22] are the most significant ones. These blends are suitable for the manufacturing of automobile and computer gears. PS has also been effectively used in packaging, building, construction, injection molding, and so on for many years. It is an amorphous polymer with a glass-transition temperature between 90 and 110°C; it has the advantages of being clear, hard, easily processable, and inexpensive. On account of the excellent properties, PS is now used in electrical and electronics parts and other industrial applications. Although PS has many desirable characteristics, its drawbacks are its low impact strength and poor chemical resistance at room temperature.[23] Conversely, aramid can be considered to be a tough material at room temperature, and it also possesses good chemical resistance. Subsequently, the blending of PS with aramid can be an expedient approach for increasing the thermal and impact strengths of PS. In this study, we predominantly studied the incorporation of polyamide in the PS matrix and its effects on PS's morphology and thermophysical properties. A new multicomponent system based on the combination of two diamines (1,5-diaminonaphthalene and 1,4-phenylenediamine) and isophthaloyl chloride (IPC) was used to compatibilize the functionalized PS. The key aspiration of this research was to elucidate the mechanism and consequences of the compatibilization of modified PS/polyamide system.

EXPERIMENTAL

Instruments

Fourier transform infrared (FTIR) spectra of thin films of polymers and blends were taken at room temperature with a resolution of 4 cm^{-1} with an Excalibur Series FTIR spectrometer (model FTSW 300 MX, Bio-Rad). The NMR spectrum was recorded at room temperature with a Bruker spectrometer operating at 300.13 MHz for ^{1}H-NMR. The solvent used for analysis was hexadeuterated dimethyl sulfoxide. Gel permeation chromatography analysis was carried out with a Waters Alliance GPCV2000 for molecular weight determination. PS was used as the standard, and dimethylformamide was used as an eluent. The eluent was monitored with a refractive index detector. The number-average molecular weight and weight-average molecular weight (M_w) were investigated. The stress–strain response of the blend samples (strips) with dimensions of about ca. 15 × 5.6–8.4 × 0.35–0.67 mm^3 was monitored according to Deutsches Institut Rir Normung procedure DIN 53455 at a crosshead speed of 5 mm/min with an Instron 4206 universal testing machine. Standard procedures and formulas were applied to calculate various tensile properties, including the stress, strain, Young's modulus, and toughness. For phase morphological studies, the specimen was plunged into liquid nitrogen and was submerged until the bubbling stopped and it was frozen. It was quickly removed by sharp-nosed tweezers. The sample was also gripped with another pair of tweezers and broken into two pieces. The sample was placed in the holder in such a way that the fractured surface was exposed for testing. The sample was then coated with a thin layer of 60/40 gold/palladium alloy with a sputtering technique. The layer deposited was 10–20 nm thick and was evenly coated on the surface of the specimen. The morphology was then investigated with an FEI Nova 230 field emission scanning electron microscope. The thermal stability of the blends was determined by a Netzsch TG 209 F3 thermogravimetric analyzer; we heated the sample in an Al_2O_3 crucible from 25 to 800°C at 10°C/min under a nitrogen atmosphere with a gas flow rate of 30 mL/min.

Materials

PS, with an M_w of 100 × 10^3 g/mol, was supplied by BDH. Anhydrous stannous chloride (98%) was obtained from Acros

Organics. Tetrahydrofuran, sodium hydroxide, nitric acid, and sulfuric acid were supplied by E-Merck (Nottingham, United Kingdom) and were used as received. Anhydrous *N,N′*-dimethylacetamide (DMAc) was procured from Aldrich. 1,5-Diaminonaphthalene, 1,4-phenylenediamine, IPC, triethylamine (TEA), ethanol, and hydrochloric acid were obtained from Fluka and were used as received.

Preparation of Aramid

The wholly aromatic polyamide was prepared by the low-temperature polycondensation of aromatic diamines and diacid chloride under anhydrous conditions. The diamines (1,5-diaminonaphthalene and 1,4-phenylenediamine) were dissolved in DMAc with their molar ratio kept at 1:1 (N_2). This mixture was cooled to 0°C; a stoichiometric amount of IPC was then added (to prevent an exothermic reaction). About 24 h was given for the completion of the reaction with constant stirring.[24] An excess of IPC was added with further stirring for 4 h to end cap the aramid with acid chloride (O═C—Cl). To remove HCl from the aramid solution, a stoichiometric amount of TEA was also added. The precipitates that formed were centrifuged, and the pure polymer was obtained with a simple decanting process. The reaction mixture was viscous and pinkish brown in color. The chemical reaction leading to the formation of the aromatic polyamide is given in Scheme 1. Gel permeation chromatography revealed an M_w of 88 × 10^3 g/mol and a polydispersity index of 2.1. The structure of the new aramid obtained was also characterized with FTIR and ^{1}HNMR analyses.

FTIR (film, υ_{max}, cm^{-1}): 3248 (N—H stretching), 1589 (N—H bending), 3012 (aromatic C—H stretching), 1674 (C═O stretching), 1502 (aromatic C═C stretching). ^{1}H-NMR (300.13 MHz, hexadeuterated dimethyl sulfoxide, δ, ppm): 6.53 (2 H_a, d), 7.14 (2 H_b, t), 7.17 (2 H_c, d), 8.57 (2 H_d, s), 8.20 (2 H_e, d), 7.62 (1H_f, t), 8.64 (1H_g, s), 6.41 (2 H_h, d), 7.42 (2 H_i, d).

Synthesis of the Amino-Functionalized Polystyrene (PS–NH_2)

PS–NH_2 was obtained in two steps, that is, nitration followed by reduction, as outlined in Scheme 2.[25] The amine functional groups introduced onto PS were actually reactive toward the acid chloride end groups of polyamide and, thus, acted as reactive compatibilizers.

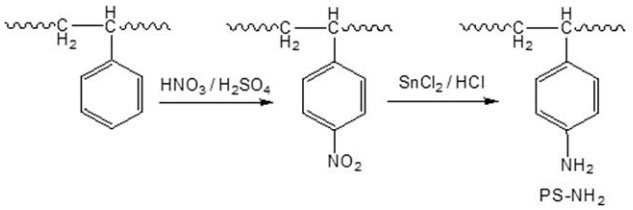

Scheme 2. Amino functionalization of PS.

Blend Preparation

Different proportions of the polyamide were blended with PS or the PS–NH_2 matrix to offer two blend systems (PS/aramid and PS–NH_2/aramid). Known amounts of the two polymers were separately dissolved in DMAc with continuous agitation to obtain a clear solution (Scheme 3). Then, these solutions were blended with constant stirring for 24 h. Thin films of the resulting blend solutions were cast in glass Petri dishes at 70°C for 36 h. Before characterization, the films were dried at 80°C *in vacuo* for 48 h to a constant weight.

RESULTS AND DISCUSSION

Spectroscopy

The spectral analyses confirmed well the expected structure of the prepared polyamide, which is illustrated in Scheme 1. The ^{1}H-NMR data were in good agreement with the proposed structure of the polymer. A downfield singlet due to the N—H proton (8.57 ppm) confirmed the formation of amide bond. The appearance of two doublets (2 H) at 6.41 and 7.42 ppm was due to the *p*-phenylene moiety. The chemical shifts (2H, doublets) at 6.53 and 7.17 and a triplet (2H) at 7.14 ppm indicated the incorporation of naphthalene functionalities in the main

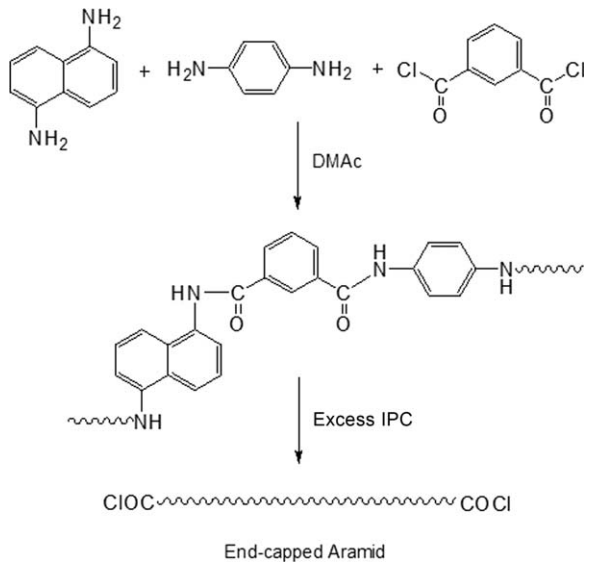

Scheme 1. Synthesis of the aramid.

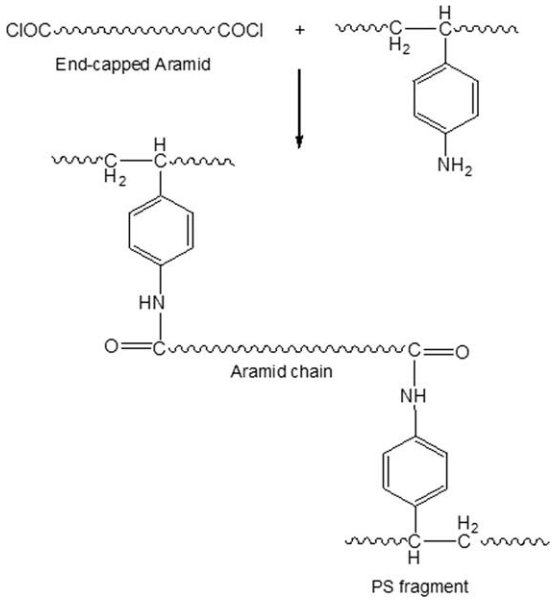

Scheme 3. Grafting of the aramid with PS–NH_2 in a compatibilized blend system.

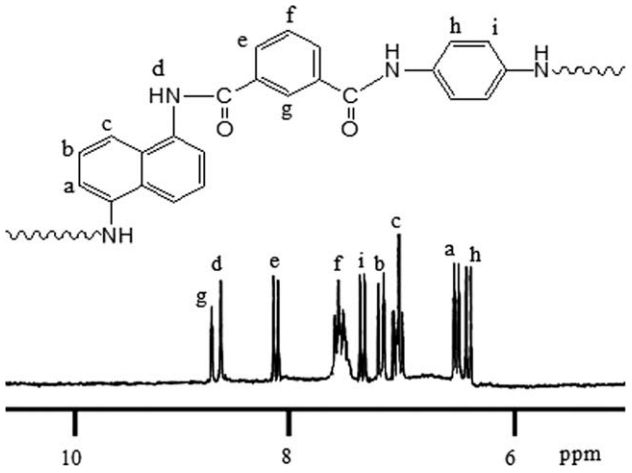

Figure 1. ^{1}H-NMR spectrum of the pure aramid.

chain. Signals for the isophthaloyl unit (1H singlet at 8.64, 2H doublet at 8.20, and 1H triplet at 7.62) further confirmed its structure (Figure 1). The FTIR spectrum of the thin-film elucidated bands at 3248 and 1589 cm^{-1} assignable to N—H stretching and bending vibrations, respectively [Figure 2(A)]. The band at 3012 cm^{-1} was attributed to the aromatic C—H, whereas C=O stretching vibrations appeared at 1674 cm^{-1}. Although there were two types of amide linkages in the polyamide structure, that is, one of the amide linkages was adjacent to *p*-phenylene, and the second linkage was near the naphthalene unit, ideally, the naphthalene amide linkage must appear at a higher wave number relative to the phenylene one. However, the appearance of a single, broad C=O stretching band at 1674 cm^{-1} showed the combined effect of both the amide bonds. Generally, in the larger and complex polymer backbone, such identical bonds are hard to locate individually compared with the spectra of monomers or oligomers. The group of closely related bands at 1500 cm^{-1} were ascribed to aromatic C=C stretching. In the FTIR spectroscopy of the PS–NH_2/aramid blend, the major peak observed was the aliphatic C—H stretching vibrations at 2913 cm^{-1} [Figure 2(B)]. However, the spectrum of pure aramid showed no vibration for aliphatic C—H stretching, but in the blend spectrum, both aromatic and aliphatic C—H bands were present. This signified the presence of PS–NH_2 chains. A band at 1662 cm^{-1} for C=O stretching was also noted. An amide linkage formed between the acid chloride end group of the aramid, and the amine group of PS–NH_2 was characterized by FTIR spectroscopy of the PS–NH_2/aramid blend. A broadening of the band due to N—H stretching in the region 3000–3300 cm^{-1} was observed. In general, the formation of N—H/C=O hydrogen bonds results in such broadening (Scheme 4). In our blend system, there were two types of amide bonds. One was present in the aramid itself, and the second was introduced by the grafting reaction between the aramid and PS–NH_2; each of these may have been hydrogen-bonded to a slightly different extent. Consequently, IR absorptions occurred at various frequencies for each of these bonds, and this resulted in the band broadening, as it was an average of all of these slightly different absorptions. Apart from these, hydrogen bonding in the PS–NH_2/aramid blend was also noticed via the appearance of carbonyls at a lower frequency (1662 cm^{-1}) relative to the pure aramid (1674 cm^{-1}). The *in situ* generation of the copolymers (PS–NH_2-grafted aramid) was thus assessed with spectroscopic analysis.

Mechanical Properties

PS/aramid and PS–NH_2/aramid blends were prepared by the addition of aramid to a PS or PS–NH_2 solution. Figure 3 illustrates the typical stress–strain behavior of the PS/aramid blends,

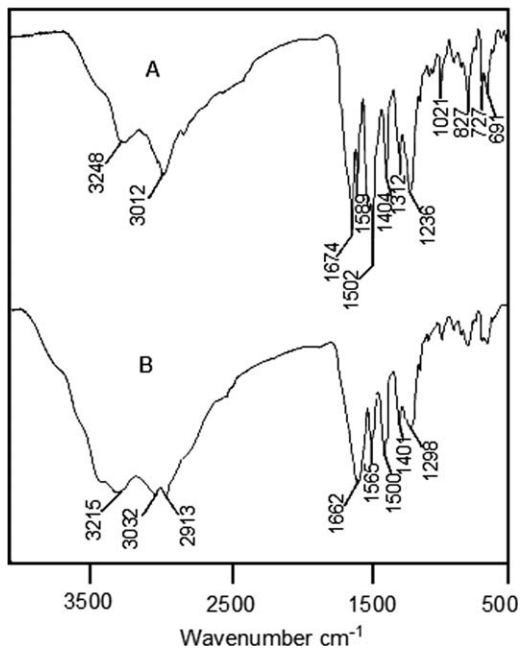

Figure 2. FTIR spectra of the (A) pure aramid and (B) PS–NH_2/aramid blend.

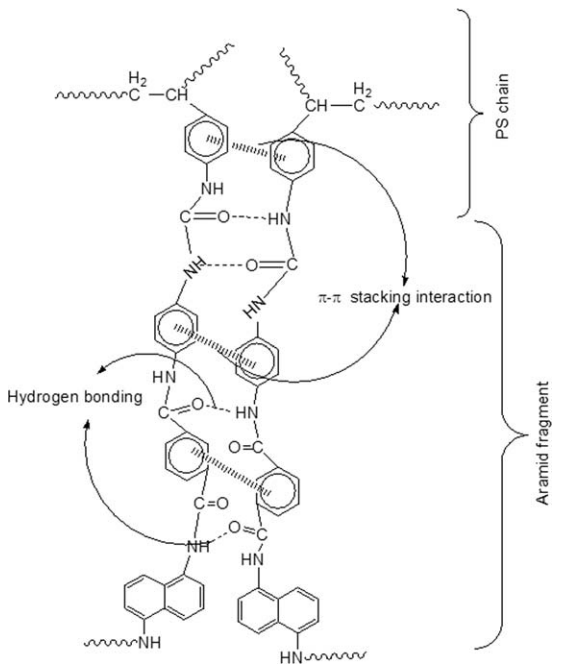

Scheme 4. Prototype representing the type of interaction between the two matrices.

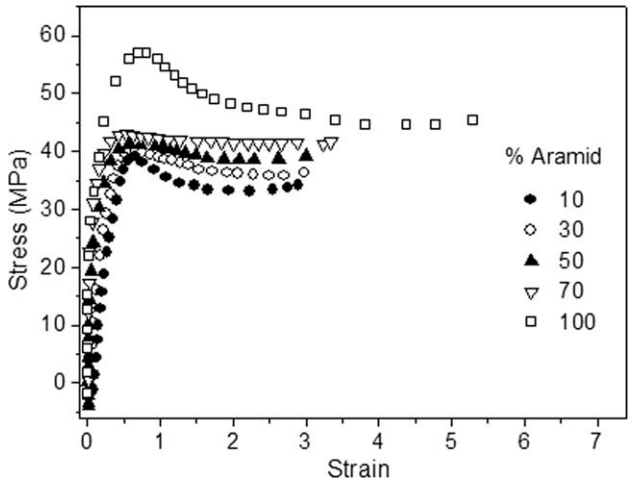

Figure 3. Stress–strain curves of the PS/aramid blends.

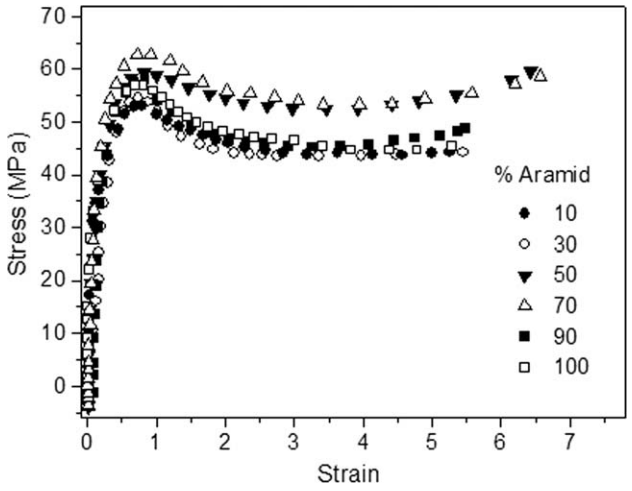

Figure 4. Stress–strain curves of the PS–NH_2/aramid blends.

and the tensile properties obtained are given in Table I. Pure PS was somewhat brittle, having a maximum stress of 12.5 MPa, but the addition of 10 wt % aramid to the PS/aramid blend increased the strength to 39.0 MPa. The maximum stress for this blend system was 41.9 MPa with 70 wt % aramid. The addition of aramid to pure PS thus resulted in an improvement in the mechanical properties with respect to PS, but the properties were poor relative to those of the neat polyamide. In all the PS/aramid blend compositions, mechanical properties were reduced relative to those of the pure polyamide. This decline in the mechanical properties demonstrated that there was weak interfacial adhesion in the uncompatibilized PS/aramid blends, which were also characterized by morphological studies representing a biphasic structure of 50 and 70 wt % aramid blends. The variation in the tensile strength in the PS–NH_2/aramid system is shown in Figure 4, and the related mechanical data is narrated in Table II. The results show an overall increase in the tensile strength relative to that of the pure aramid. The ultimate stress at break for these materials increased with increasing aramid concentration. The addition of aramid up to 30 wt % in the PS/aramid blends increased the ultimate stress at break to 54.4 MPa. Upon the further addition of aramid, the tensile strength increased markedly. The maximum value for stress was observed for the 70 wt % aramid composition (62.7 MPa) in this blend system. Moreover, the pure aramid had a maximum strain value of 5.29, which also increased to 6.57 with 70 wt % aramid. The modulus values demonstrated that the pure aramid had a value of tensile modulus of 1.55 GPa, which increased with the addition of 50 wt % aramid in PS–NH_2 (1.60 GPa) and reached a maximum for the 70 wt % loading (1.74 GPa). However, the tensile modulus of the blend containing 30 wt % aramid was 1.18 GPa, which was less than that of pure polyamide. The toughness of the blend with 10 wt % aramid depicted a value of 237.0 MPa and then increased up to a 70 wt % polyamide content (362.6 MPa). The addition of aramid to the PS–NH_2 matrix resulted in an improvement in the mechanical properties. Both the aramid and PS–NH_2 were amorphous in nature. The functional PS chains thus could penetrate into the aramid chains to form close packing. The spectral and morphological analyses also depicted an *in situ* reaction between acid chloride end groups (aramid) and amine functionalities (PS–NH_2) to render a fine dispersion of the two phases (Scheme 3). The chemical reaction between the PS–NH_2 and aramid resulted in a microdomain structure (interface) that transferred stress from PS to the aramid phase. This development of the PS–NH_2-grafted aramid copolymer was expected to supplement the compatibility between the aramid and functionalized PS phase. The chemical coupling of the acid chloride end-capped aramid and PS–NH_2 demonstrated a better mechanical profile than the uncompatibilized PS/aramid blends. PS–NH_2 thus behaved as a blend compatibilizer (*in situ* copolymer formation) to form miscible nanoblends.

Table I. Mechanical Properties of the PS/Aramid Blends

Aramid (%)	Maximum stress ± 2.0 (MPa)	Maximum strain ± 0.02 (%)	Initial modulus ± 0.02 (GPa)	Toughness ± 3.0 (MPa)
0	12.5	0.03	0.75	0.16
10	39.0	2.89	0.28	100.4
30	39.9	2.96	0.30	105.8
50	40.4	3.00	0.56	108.2
70	41.9	3.33	0.83	136.7
100	55.1	5.29	1.55	250.1

Table II. Mechanical Properties of the PS–NH_2/Aramid Blends

Aramid (%)	Maximum stress ± 2.0 (MPa)	Maximum strain ± 0.02 (%)	Initial modulus ± 0.02 (GPa)	Toughness ± 3.0 (MPa)
0	13.1	0.02	0.94	1.1
10	53.0	5.30	1.02	237.0
30	54.4	5.45	1.18	239.9
50	60.0	6.42	1.60	345.7
70	62.7	6.57	1.74	362.6
90	57.9	5.48	1.08	255.6
100	55.1	5.29	1.55	250.1

Microscopic Study

Figure 5 compares field emission scanning electron microscopy (FESEM) images for the blends of uncompatibilized PS/aramid. These samples were unable to form graft copolymers but actually formed homopolymer blends without any chemical linking between the two phases. They clearly showed a phase-separated structure, which included aramid large domains in the PS matrix as immiscible homopolymer blends. This was probably because of the aggregation of PS (self-association), which in turn, induced the segregation of the aramid homopolymer from a regular structure.[26,27] The FESEM images for the PS–NH_2/aramid blends are displayed in Figures 6–8. The micrographs show that PS was a brittle polymer and acted as a matrix dark portion, whereas aramid was present as a second phase spread between the dark portions. Figure 6(A) (10 wt % aramid) showed a comparatively nanophase-separated structure of the aramid domain in the PS–NH_2 matrix. The plastic deformation of the matrix in the vicinity of the dispersed aramid phase formed white regions during the cryofracture of the specimen surface [Figure 6(B,C)]. Such a type of morphology is often observed in systems of high interfacial adhesion. To examine the two-phase morphology clearly, etching analysis was performed. Etching is a handy method for the preferential dissolution of the organic matrix to (1) provide three-dimensional relief of the polished surface, (2) enhance the contrast between dissimilar and discontinuous zones for better identification, and (c) enhance accretion zones for scanning electron microscopy examination, which may permit fine resolution.[28] The ultimate objective of etching was to provide a consistent relief pattern throughout the section and limit artifact formation. First, the fractured sample was placed in a glass beaker, and etching solutions [2 mL of HCl (59%) and 2 mL of ethylene diamine tetraacetic acid (23%)] were poured gently to the section with a pipette. After a short length of time (10 min), the solution was removed, and deionized water was added. After etching, the white region appearing due to plastic deformation of the matrix disappeared, and the matrix appeared as a continuous phase in the 30 wt % aramid blend sample. Figure 6(E) helps to build a comparative analysis for the sample morphology before and after etching. Consequently, the white regions were found to appear because of the plastic deformation of PS. The addition of the 40 wt % aramid [Figure 6(D)] brought about some rearrangement of both of the phases. Further inclusion of the aramid initiated the self-assembly process to form nanoblends. Afterward, in the 50 wt % aramid blend [Figure 7(A)], polyamide, along with the functional PS, formed a well-knitted self-assembled nanoframe work. When the fraction of aramid was increased to 60 wt % [Figure 7(B)], a very unique self-assembled nanostructure was observed. Upon further loading of aramid (70 wt %), a fine, distinctive, and cocontinuous self-assembled morphology was

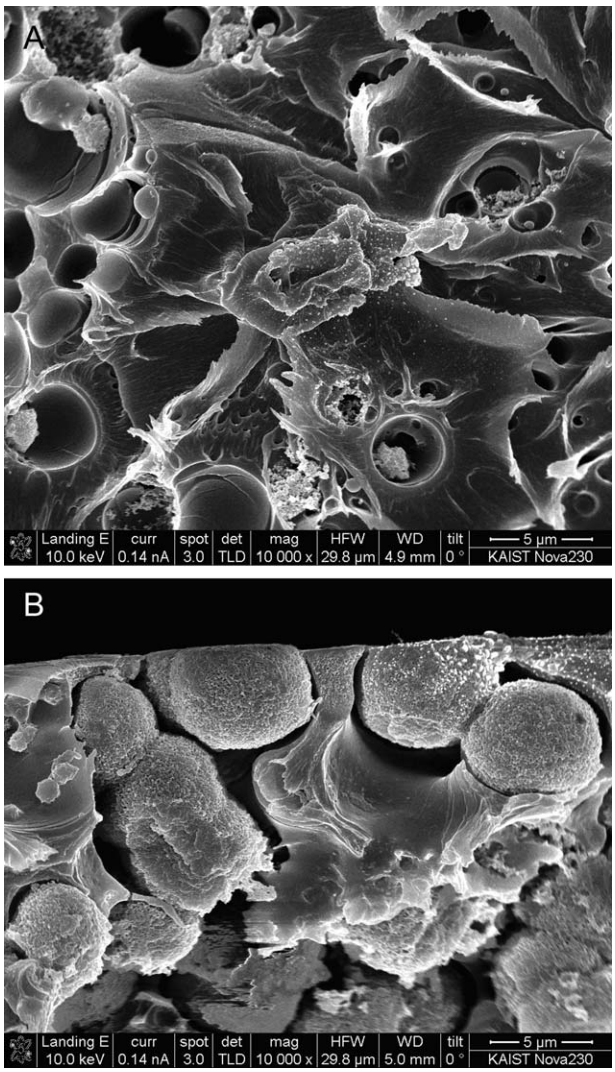

Figure 5. FESEM micrographs of the PS/aramid blends with (A) 50 and (B) 70 wt % aramid.

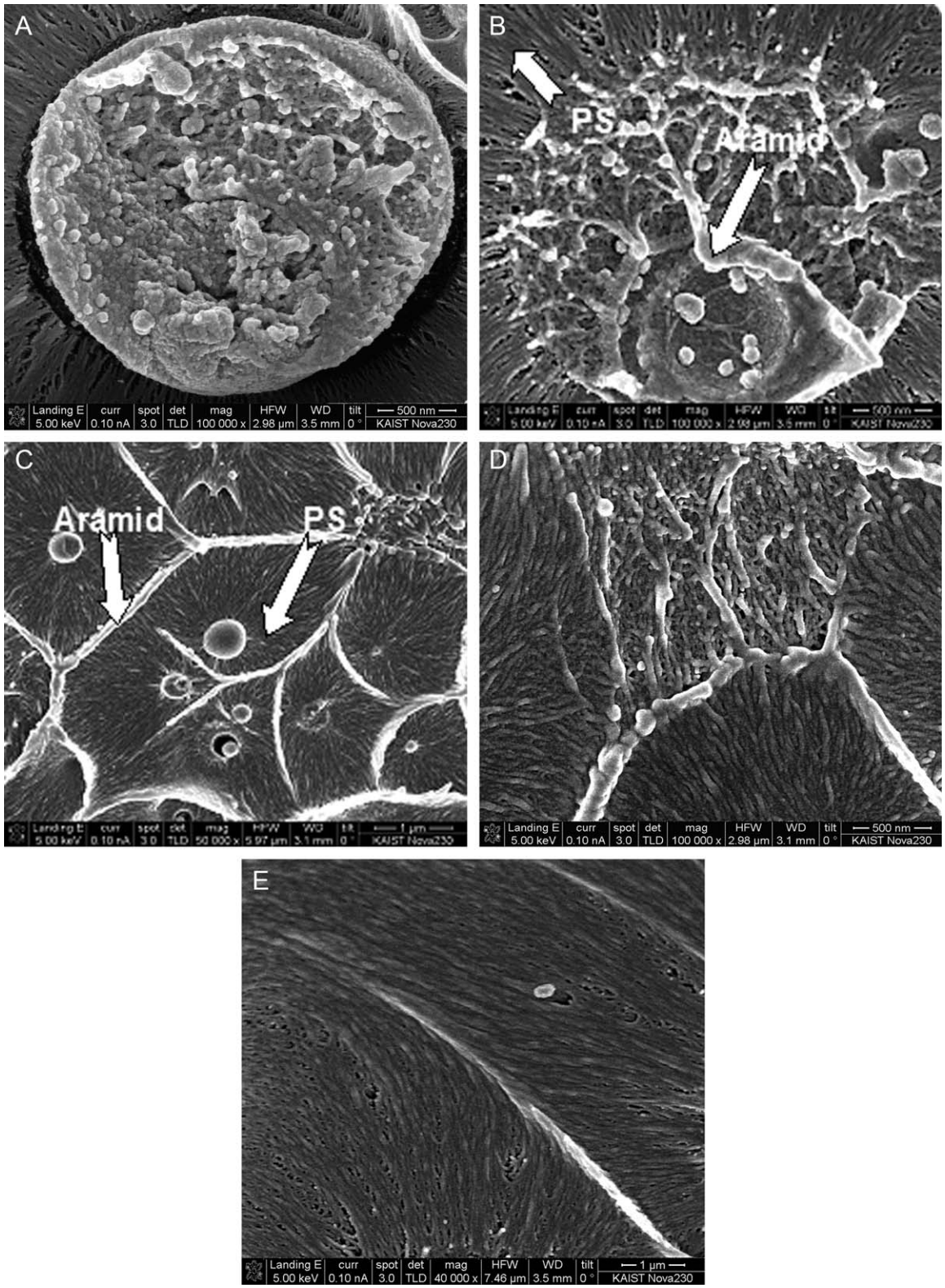

Figure 6. FESEM micrographs of the PS–NH_2/aramid blends with (A) 10, (B) 20, (C) 30, (D) 40, and (E) 30 wt % aramid after etching.

fashioned by the two polymers [Figure 7(C)]. The nanostructured morphology was accompanied by good ordering and orientation. There was a slightly less prearranged nanomorphology in the 80 and 90 wt % aramid blends [Figure 8(A,B)]; therefore, phase separation was observed. The macrophase separation was thus not observed above a 30 wt % aramid composition in the

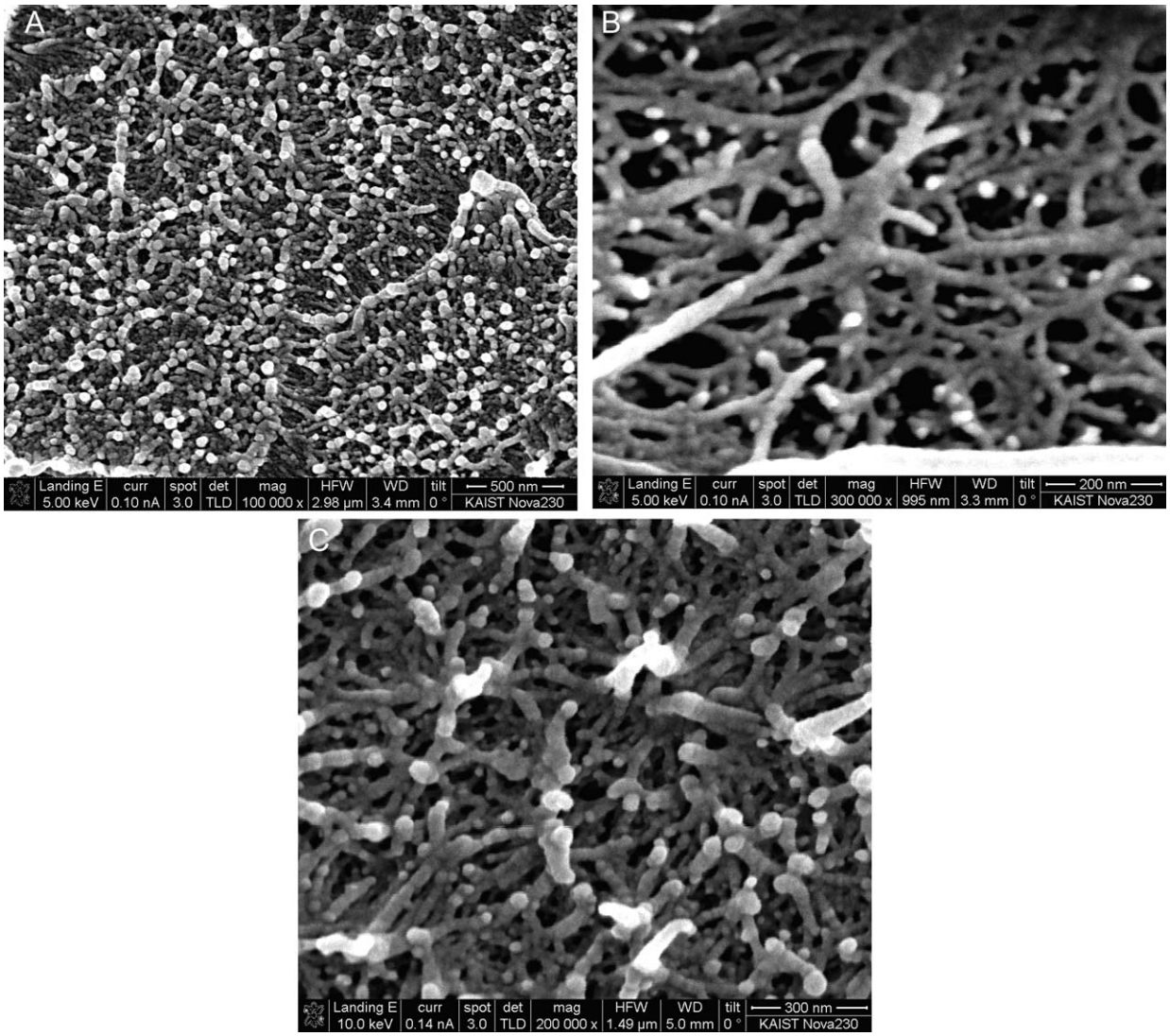

Figure 7. FESEM micrographs of the PS–NH_2/aramid blends: (A) 50, (B) 60, and (C) 70 wt % aramid.

PS–NH_2/aramid system, and this was in contrast to the results for the PS/aramid blends. There was also a significant correspondence between the mechanical properties and the morphologies of the blends. In the PS–NH_2/aramid system, the three types of competitive interactions derived a well-defined molecular self-assembly: (1) hydrogen bonding (N—H/C═O), (2) π–π stacking interactions among phenyl units, and (3) chemical linking between the amine and acid chloride functionalities of the blend components.[29,30] The chemical interaction in the PS–NH_2/aramid system occurred spontaneously at the interface between the two polymers in the solution. The introduction of the reactive groups in the PS–NH_2/aramid system; this resulted in a substantial reinforcement of the interface. The adhesion continued to improve as the amount of aramid increased. The π–π stacking interactions in addition to intermolecular interactions further strengthened the nanostructure. The compatibilized system yielded self-assembled nanoblends relative to the uncompatibilized system. Here, we investigated the composition-dependent morphological variation in the PS–NH_2/aramid and PS/aramid blends. Because of the simplicity of synthesis and the high yield of the graft copolymer, this approach could be efficiently used to produce self-assembled nanostructured templates for ensuing nano-applications.

Thermal Stability

The extent of compatibility between the phases was evaluated by thermal degradation and the glass-transition temperature. The weight loss temperatures of the PS/aramid and PS–NH_2/aramid blends were investigated by means of thermogravimetric analysis (Table III). The thermograms of the PS/aramid and PS–NH_2/aramid blends are presented in Figures 9 and 10, respectively. From the thermograms, the initial decomposition temperature (T_0) and the temperature at 10% gravimetric loss (T_{10}) were determined. The thermal data revealed that the PS–NH_2-based blend containing 10 wt % PS–NH_2 had superior thermal stability ($T_0 = 375°C$, $T_{10} = 419°C$) relative to the 10 wt % PS/aramid blend ($T_0 = 328°C$, $T_{10} = 400°C$). This signified that the grafting of the aramid chains on the functional PS enhanced the heat stability of the blends. Additionally, the residual weights observed at 700°C for the 10 wt % PS–NH_2/aramid

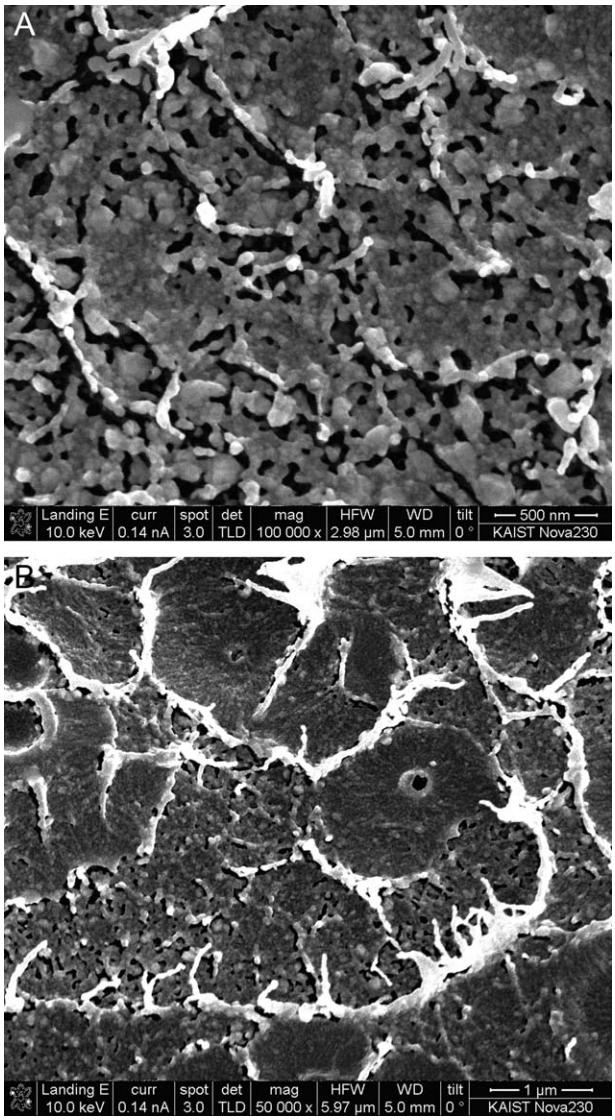

Figure 8. FESEM micrographs of the PS–NH_2/aramid blends: (A) 80 and (B) 90 wt % aramid.

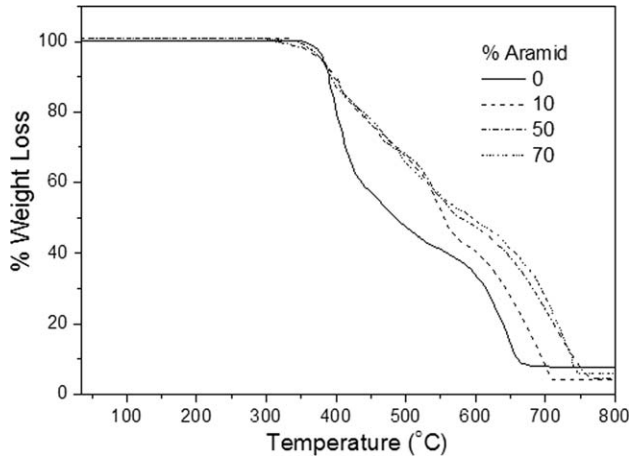

Figure 9. Thermograms of the PS/aramid blends at a heating rate of 10°C/min in N_2.

and PS/aramid blends were found to be 11 and 13%, respectively. T_{10} of the 50 wt % PS–NH_2/aramid blend was 431°C, whereas the PS/aramid blend showed decomposition at a lower temperature (350°C). Similarly, the char yield (Y_c) for the 50 wt % aramid system for the PS–NH_2/aramid and PS/aramid blends was 22 and 16% (700°C). T_0 and T_{10} were found to be 444 and 490°C for the 70 wt % PS–NH_2 blend. With the inclusion of aramid in the PS–NH_2/aramid system, there was a clear increase in T_{10} [419°C (10 wt %)] to [490°C (70 wt %)]. The thermogravimetric results undoubtedly demonstrate that the pure PS-based blends were thermally less stable than the amino-functional blends. Moreover, we predicted that the functionalized PS blends were much more compatible than the pure PS ones. Though, only an opposite amount of the two phases offered enhanced compatibility and unique morphology, such as the 70 wt % aramid containing PS–NH_2 blend. Miscibility was achieved by virtue of the greater interfacial bonding between the two phases. Novel nanoblends of the functionalized PS also displayed better thermal and morphological characteristics compared to the reported PS blends.[25,31]

Table III. Thermal Analysis Data for the Blend Systems

Blend system	Aramid (%)	T_0 (°C)	T_{10} (°C)	Y_c at 700°C (%)[a]
PS/aramid	0	370	398	9
	10	328	400	11
	50	350	402	16
	70	363	403	17
PS-NH_2/aramid	0	350	388	10
	10	375	419	13
	30	407	462	12
	50	431	481	22
	70	444	490	28
	100	445	491	51

[a] Weight of polymer remaining.

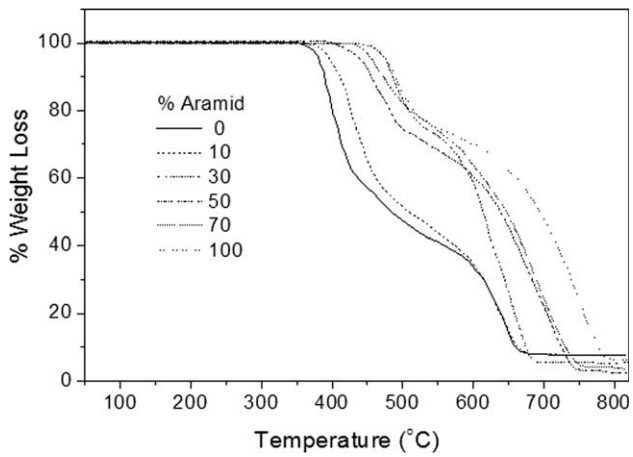

Figure 10. Thermograms of the PS–NH_2/aramid blends at a heating rate of 10°C/min in N_2.

CONCLUSIONS

In this study, we aimed to investigate a new approach toward self-assembly in *in-situ* grafted copolymer blends. PS–NH_2 chains contributed toward the *in situ* formation of the aramid-grafted PS–NH_2 copolymer because of the chemical linking of modified PS and acid chloride functional aramid. A comparative account, in morphological, thermal, and mechanical facets, was contemplated for the compatibilized and uncompatibilized PS–NH_2/aramid systems. Unique self-assembled nanostructured blends were perceived for the functionalized PS blends with various aramid contents when compared with the unmodified PS system. The morphological divergence between the two series was believed to be the result of the reactive compatibilization and physical linking of the components in the compatibilized system. The exceptional morphology may unlock several applications of PS–NH_2/aramid blends formerly unattainable to neat PS. Furthermore, the thermal stability of the compatible blends demonstrated a significant increase with respect to the PS/aramid blends. Conclusively, the unique mechanical, thermal, and morphological properties related to the self-assembly were anticipated for these nanostructured blends. Obviously, the formation of the graft copolymer contributed to the enhanced compatibility of the binary blends and, as a result, improved the mechanical, thermal, and morphological properties. In this way, we developed new self-assembled structures with a graft copolymer possessing potential relevance in wide variety of nanotemplate materials.

ACKNOWLEDGMENTS

One of the authors (A.K.) gratefully acknowledges the Higher Education Commission of Pakistan for its financial support of this work under the International Research Support Initiative Program and Indigenous 5000 Ph.D. Fellowship Scheme Batch III (contract grant number 063–111354-Ps3–068).

REFERENCES

1. Xia, Y. N.; Rogers, J. A.; Paul, K. E.; Whitesides, G. M. *Chem. Rev.* **1999**, *99*, 1823.
2. Marrian, C. R. K.; Tennant, D. M. *J. Vac. Sci. Technol.* **2003**, *21*, S207.
3. Ducharme, S.; Gruverman, A. *Nat. Mater.* **2009**, *8*, 9.
4. Bates, F. S.; Fredrickson, G. H. *Phys. Today* **1999**, *52*, 32.
5. Matyjaszewski, K.; Muller, A. H. E. *Prog. Polym. Sci.* **2006**, *31*, 1039.
6. Bates, F. S. *Science* **1991**, *251*, 898.
7. Macaubas, P. H. P.; Demarquette, N. R. *Polymer* **2001**, *42*, 2543.
8. Sciamanna, R.; Arribas, G.; Albano, C.; Horie, E.; Soto, B. *Mater. Res. Innovat.* **2001**, *4*, 311.
9. Böltau, M.; Walheim, S.; Mlynek, J.; Krausch, G.; Steiner, U. *Nature* **1998**, *391*, 877.
10. Pernot, H.; Baumert, M.; Court, F.; Leibler, L. *Nat. Mater.* **2002**, *1*, 54.
11. Pimbert, S.; Avignon-Poquillon, L.; Levesque, G. *Polymer* **2002**, *43*, 3295.
12. Zhang, L. *Eur. Phys. Lett.* **2011**, *93*, 58002.
13. Webber, S. E. *J. Phys. Chem. B* **1998**, *102*, 2618.
14. Flory, P. J. *J. Chem. Phys.* **1942**, *10*, 51.
15. Huggins, M. L. *J. Phys. Chem. B* **1942**, *46*, 151.
16. Matsen, M. W. *J. Chem. Phys.* **1997**, *106*, 7781.
17. Abetz, V. Block Copolymers II; Springer: New York, **2005**; Vol. *189*, p 125.
18. Halimatudahliana, I. H.; Nasir, M. *Polym. Test.* **2002**, *21*, 163.
19. Hameed, N.; Thomas, S. P.; Abraham, R.; Thomas, S. *Exp. Polym. Lett.* **2007**, *1*, 345.
20. Hamley, I. W. The Physics of Block Copolymers; Oxford University Press: New York, **1998**; p 122.
21. Segalman, R. A. *Mater. Sci. Eng. R* **2005**, *48*, 191.
22. Szwarc, M. *Nature* **1956**, *178*, 1168.
23. Birley, A. W.; Haworth, B.; Batchelor, J. General Chemical Resistance (Physics of Plastics); Hanser: New York, **1992**; p 488.
24. Zulfiqar, S.; Sarwar, M. I. *High Perform. Polym.* **2009**, *21*, 3.
25. Shabbir, S.; Zulfiqar, S.; Ahmad, Z.; Sarwar, M. I. *Polym. Eng. Sci.* **2008**, *48*, 1793.
26. Bates, F. S.; Maurer, W. W.; Lipic, P. M.; Hillmyer, M. A.; Almdal, K.; Mortensen, K.; Fredrickson, G. H.; Lodge, T. P. *Phys. Rev. Lett.* **1997**, *79*, 849.
27. Singh, S.; Rao, C. N. R. *J. Phys. Chem.* **1967**, *71*, 1074.
28. Yang, M.; Cao, K.; Sui, L.; Qi, Y.; Zhu, J.; Waas, A.; Arruda, E. M.; Kieffer, J.; Thouless, M. D.; Kotov, N. A. *ACS Nano* **2011**, *5*, 6945.
29. Jiang, G.; Wang, L.; Chen, T.; Yu, H.; Wang, C.; Chen, C. *Polymer* **2005**, *46*, 5351.
30. Jiang, G.; Wang, L.; Chen, T.; Dong, X.; Yu, H.; Wang, J.; Chen, C. *J. Polym. Sci. Part A: Polym. Chem.* **2005**, *43*, 5554.
31. Xu, S.; Tang, T.; Chen, B.; Huang, B. *Polymer* **1999**, *40*, 2081.